npj | climate and atmospheric science

Article

Published in partnership with CECCR at King Abdulaziz University

https://doi.org/10.1038/s41612-024-00756-5

Insight into wet scavenging effects on sulfur and nitrogen containing organic compounds in urban Beijing

Chunyan Zhang[1,2,3], Yonghong Wang[2] ✉, Jun Liu[2], Tianzeng Chen[2], Wei Huang[4], Zirui Liu[5], Biwu Chu[2], Qingxin Ma[2,3] & Hong He[1,2,3] ✉

Sulfur-containing organic compounds (SOCs) and nitrogen-containing organic compounds (NOCs) play critical roles in regulating the physical and chemical properties of organic aerosols (OA), while the understanding of them remains limited. Here, the high-resolution real-time measurements of submicron aerosols were conducted in urban Beijing, mainly to investigate wet scavenging effects on the potential formation and evolution mechanism of OA, especially SOCs and NOCs. OA composition transitioned from being primarily SOCs before wet processes to NOCs after wet processes. Further molecular fragments identification suggested SOCs mainly comprised glycolic acid sulfate formed by aqueous-phase processing during the entire observation, and aromatic- and monoterpene-derived SOCs formed by photochemical processing before snowfall. NOCs species were diverse and dominated by highly oxidized amides and amino acids mainly produced by photochemical processing. This study provided an in-depth insight into the potential formation and evolution pathways of SOCs and NOCs in OA in the urban atmosphere.

Winter haze pollution, caused by a severe excess of submicron aerosol (PM_1), remains a challenge for improving air quality in the North China Plain (NCP)[1–4]. Numerous real-time field observations have been conducted to investigate the chemical composition, sources, formation pathways, and ageing process of PM_1 in severe haze episodes of NCP, particularly in a typical megacity like Beijing[5–10]. Organic aerosols (OA) are normally the most abundant component in PM_1, accounting for 31–59% of PM_1 mass concentration during winter haze periods[8,11–13]. Nevertheless, the chemical composition of OA at the molecular level, as well as its formation and ageing process still remain unclear, especially secondary organic aerosol (SOA), which accounts for about 43–78% of OA in various Asian sites[12].

SOA can be formed through atmospheric oxidation of volatile organic compounds (VOCs)[14–18], as well as generated from the oxidation of primary OA (POA) on wet particles or fog/cloud droplets[16,19,20]. Extensive studies have suggested that photochemical oxidation reactions played an important role in the formation of less-oxidized oxygenated OA (LO-OOA), while aqueous-phase processing was dominated by the formation of more-oxidized oxygenated OA (MO-OOA)[8,21,22]. Zhan et al. [20] proposed that the evolution of LO-OOA through photochemical oxidation also can contribute to the formation of MO-OOA. Xiao et al. [11] suggested SOA formation also can be promoted by photochemical aqueous-phase oxidation. The diverse of SOA formation pathways highlighted the importance of analyzing its formation characteristics along with detailed precursors and meteorological factors.

Sulfur-containing organic compounds (SOCs) and nitrogen-containing organic compounds (NOCs) are ubiquitous constituents of OA and serve as important tracers for SOA with great abundance and species diversity. Glycolic acid sulfate (GAS) derived from the aqueous uptake of glyoxal on sulfate aerosols constitutes a significant portion of SOCs in Beijing[23,24]. Additional organosulfates formed by anthropogenic polycyclic aromatic hydrocarbons (PAHs) and aromatic compounds, as well as by biogenic monoterpene and isoprene through •OH-, $•NO_3$- and O_3-initiated oxidation[25–27] also contributed significantly to SOCs mass loading in urban aeras[28–30]. For NOCs, gas-phase NOCs species have been measured by NO_3^- time-of-flight chemical ionization mass spectrometer (NO_3^--ToF-CIMS) and most of the oxygenated organic molecules with nitrogen contribute to a significant fraction of OA via gas to particle conversion[17,31]. Koenig et al. [32] observed particulate organic nitrogen and defined nitrophenols and monoterpene-

[1]Center for Excellence in Regional Atmospheric Environment, Institute of Urban Environment, Chinese Academy of Sciences, Xiamen, China. [2]State Key Joint Laboratory of Environment Simulation and Pollution Control, Research Center for Eco-Environmental Sciences, Chinese Academy of Sciences, Beijing, China. [3]University of Chinese Academy of Sciences, Beijing, China. [4]State Key Laboratory of Loess Science, Institute of Earth Environment, Chinese Academy of Sciences, Xi'an, China. [5]Institute of Atmospheric Physics, Chinese Academy of Sciences, Beijing, China. ✉e-mail: yonghongwang@rcees.ac.cn; honghe@rcees.ac.cn

derived NOCs in Beijing. Garmash et al.[33] obtained gaseous nitrophenol-type compounds formed by •OH oxidation of aromatic compounds and NOx (=NO + NO_2) in chamber experiments. Besides, organonitrates can be generated from the oxidation of alkanes and olefins by •OH- and •NO_3-initiated processes in the presence of NOx during daytime, as well as through reactions between •NO_3 and olefins during nighttime[34–36]. Although SOCs and NOCs have been identified and resolved through a combination of laboratory studies and field observations, there is still a lack of study at the molecular level, resulting in a limited understanding of the atmospheric formation mechanisms and evolution process of SOCs and NOCs. Precipitation in the atmosphere is supposed to remove most of the gas and aerosol via wet scavenging, which has the ability to prevent the formation of SOCs and NOCs from precursors and reaction conditions.

In this study, we carried out high-resolution real-time measurements of submicron aerosol species and related gaseous precursors from 1st October to 12th November 2021 in downtown Beijing. The observation site was surrounded by well-developed traffic and dense residential areas. Here, we comprehensively investigated and compared the chemical compositions distribution of OA, particularly SOCs and NOCs, as well as their source apportionment, formation mechanisms, evolution process before and after two wet scavenging processes.

Results and discussion

Overview of the observation

The time series of non-refractory PM_1 (NR-PM_1) species concentration, related parameters (including gas species, meteorological parameters, and aerosol properties), and estimated SOCs and NOCs mass concentrations were exhibited in Fig. 1 and Supplementary Fig. 1. The mass concentration of NR-PM_1 ranged from 0.9–96.6 μg m^{-3} with average values of 46.9 ± 18.3 μg m^{-3} in haze period, 6.9 ± 7.4 μg m^{-3} in clean period, and 19.2 ± 21.8 μg m^{-3} in entire observation period. The estimated mass concentration of SOCs ranged from 0.01 to 1.45 μg m^{-3} in the haze period, with a maximum fraction of 10% in OA and 14% in total particulate sulfur (=SO_4^{2-} + SOCs). NOCs exhibited the estimated mass concentration range from 0.07 to 0.80 μg m^{-3} in the haze period, with OA contributing up to 4% and total particulate nitrogen (=NO_3^- + NH_4^+ + NOCs) accounting for 10%.

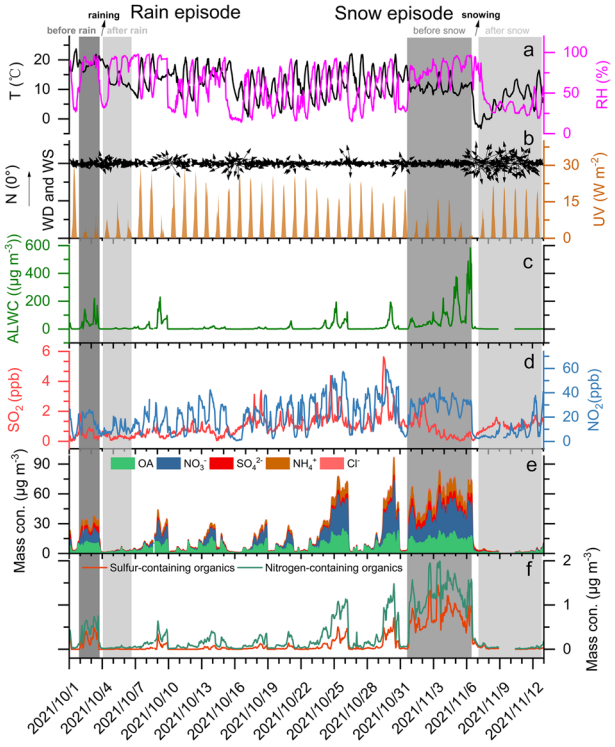

Fig. 1 | Time series of meteorology parameters and chemical species. **a** Temperature and relative humidity, **b** Wind direction, wind speed, and UV irradiation intensity, **c** Aerosol liquid water content (ALWC), **d** SO_2 and NO_2 concentrations, **e** Mass concentrations of OA, sulfate, nitrate, ammonium, and chloride, **f** Mass concentrations of sulfur-containing organic compounds (SOCs) and nitrogen-containing organic compounds (NOCs). Shaded areas indicate two precipitation episodes, and text labeling is provided before and after rain and snow, respectively; middle blank is the precipitation period, with the rain event lasting ~9 h and the snow event lasting ~20 h.

Two wet scavenging processes were determined during the observation period, namely rain episode and snow episode, as indicated by the shaded areas in Fig. 1. The darker shading represents the period before precipitation, while the lighter shading indicates the period after precipitation. The average mass concentrations of NR-PM_1 were 26.5 ± 8.2 μg m^{-3} and 2.5 ± 1.1 μg m^{-3} before and after rain, and 54.5 ± 13.4 μg m^{-3} and 2.3 ± 1.6 μg m^{-3} before and after snow, respectively (Supplementary Table 1). The results suggested that wet scavenging episodes can dramatically remove atmospheric particulate matters (PM), with a wet scavenging efficiency of > 90% for NR-PM_1. Besides, the SOCs average mass concentrations were 0.24 ± 0.14 μg m^{-3} and under detection limit before and after rain, and 0.78 ± 0.25 μg m^{-3} and 0.01 ± 0.01 μg m^{-3} before and after snow, respectively. For NOCs, the averaged mass concentrations of 0.22 ± 0.06 μg m^{-3} and 0.03 ± 0.01 μg m^{-3} were observed before and after rain, respectively. Its average mass concentrations were 0.51 ± 0.10 μg m^{-3} and 0.03 ± 0.002 μg m^{-3} before and after snow, respectively. The wet scavenging efficiency of SOCs can achieve 99%, while that of NOCs was between 85%–95%. Before rain, the haze event was accompanied by accumulated trace gases, weakened solar radiation, rising ALWC (53.7 ± 49.0 μg m^{-3}, with the maximum value of 219.4 μg m^{-3}), which were conducive to aqueous-phase reactions. After rain, PM were removed and both gases and ALWC decreased. The distribution of PM and related meteorological factors of snowfall events was similar to the rainfall process, with the exception that the period before the snow was preceded by near-stationary wind speed (0.5 m s^{-1}), as well as the elevated solar radiation and O_x (=O_3 + NO_2, Supplementary Fig. 1) during the day on the 3rd and 4th November, which was conducive to photochemical reactions. Therefore, the haze events before rain and snow should have different pathways for PM accumulation.

In addition, the transport of air masses before and after two wet scavenging episodes was analyzed by backward trajectory and shown in Supplementary Fig. 2. During the rain episode, the medium- and long-distance transport of air masses came from northwest Mongolia, accounting for ~50%, and the short-distance transport came from the east and northeast. However, apparent differences in sources of air masses were existed before and after snowfall. Before snowfall, 78% of air masses were from local sources; medium- and long-distance transport came from the northwest with 7% and 4%, respectively; and short-distance transport came from the northeast (7%) and southeast (4%). After snowfall, air masses predominately came from medium- and long-distance transport in the northwest direction. Air masses from the locality and the south of Beijing are typically with higher loadings of aerosols and precursors, while those from the northwest and north are relatively clean. This corresponded to the evolution of NR-PM_1 loadings during two precipitation periods.

OA evolution before and after wet scavenging

As shown in Fig. 2, wet scavenging had significant impact on the decline of NR-PM_1, OA, SOCs, and NOCs, especially in the snow episode with scavenging efficiencies of 96%, 91%, 99%, and 95%, respectively. Figure 2a showed the mass fraction of components of NR-PM_1, and OA constituted the large proportion of NR-PM_1 during haze and clean periods (29% and 52%, respectively), which was consistent with previous measurements in Beijing (31–59%)[37–40]. The proportions of OA during clean periods were highest, which was up to 68% after rain. This implied that wet scavenging was committed to changing the fine particulate matters from inorganic- to organic-dominance since the powerful cleaning of inorganics (95–98%) and their precursors (such as SO_2 and NO_2 in Fig.1d) by precipitation.

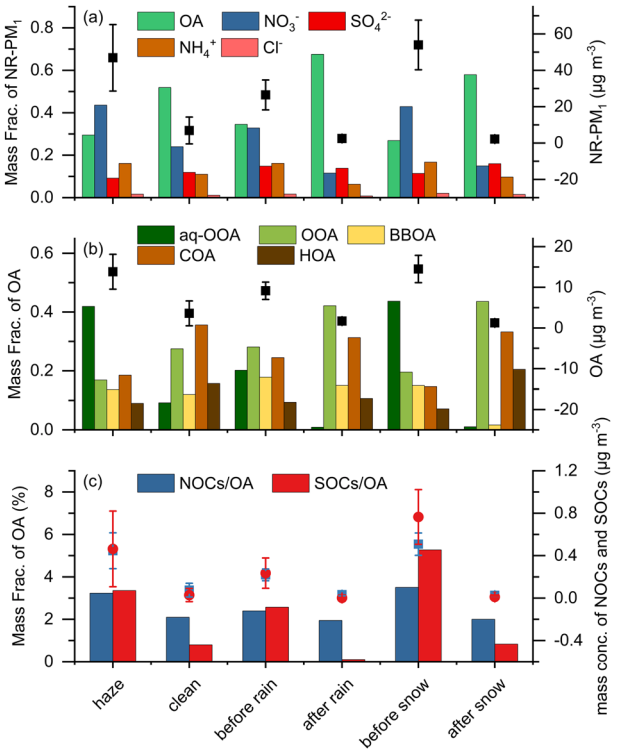

Fig. 2 | Average proportion and concentration of chemical compositions. a NR-PM_1 (OA, sulfate, nitrate, ammonium, and chloride), **b** OA (aq-OOA, OOA, BBOA, COA, and HOA), **c** Sulfur-containing organic compounds (SOCs) and nitrogen-containing organic compounds (NOCs) in haze, clean, before and after rain, and before and after snow during observation, respectively. For concentrations of NR-PM_1, OA, and NOCs, and SOCs, the solid points of the square or circle are the mean values, and the upper and lower edge lines are plus and minus one standard deviation.

OA was classified as two SOA (oxygenated OA (OOA), and aqueous-phase related OOA (aq-OOA)), and three POA (hydrocarbon-like OA (HOA), cooking-related OA (COA), and biomass burning OA (BBOA)) factors by Positive Matrix Factorization (PMF) analysis (See Supplementary Note 1 for detailed analysis). As shown in Fig. 2b, the composition of OA was considerable various that SOA dominated the OA components in the haze period (59%), and POA dominated in the clean period (63%). aq-OOA and OOA accompanied by a higher degree of ageing accounted for the highest proportion before the rain (20% and 28%) and snow (44% and 20%), while COA and HOA with low oxidation degree had higher proportions after rain (31% and 11%) and snow (33% and 21%). This suggested that the oxidation degree of atmospheric particles was higher before wet scavenging processes, and aqueous-phase oxidation processing dominated the evolution of the atmospheric particles during the haze period. However, the proportion of BBOA decreased after precipitation, which was attributed to the effective removal of long-range transported BBOA by strong wind (Fig. 1b) and related feature fragments by wet scavenging (Supplementary Fig. 3c). In contrast to the decline of BBOA proportion, the proportions of COA and HOA rose after precipitation, particularly COA, indicating that stable local sources of cooking from surrounding dense residential areas. Therefore, wet scavenging promoted the transformation of OA aerosol from SOA-led to POA-led. The transformation was primarily due to stable primary emissions (COA and HOA) and weakened favorable meteorological factors for SOA formation (low ALWC) after precipitation.

Lastly, the proportions of SOCs and NOCs to OA were compared. The results exhibited that the SOCs proportion was greater than that of NOCs during the haze period, while the opposite result was obtained during the clean period. It was significantly stated that the scavenging rates of SOCs were higher than those of NOCs, with rates of 99% and 85% during rain episode, and 99% and 95% during snow episode, respectively. Meanwhile, the mass concentrations of SOCs and NOCs were in line with the proportional change trend. Hence, wet scavenging gave rise to alternating dominance of SOCs and NOCs. This can be attributed to the robust removal of SOCs by wet scavenging and favorable conditions for the generation of NOCs after precipitation (sufficient UV radiation (Fig. 1b), abundant NO_X and O_3 (Supplementary Fig. 1)).

Analysis of SOCs and NOCs before and after wet scavenging

As depicted in Fig. 3a, the ratio of SO_2^+/SO^+ exhibited minimal change with RH, whereas the ratio of $SO_2^+/H_2SO_4^+$ sharply increased with RH. Given that ammonium sulfate (AS) can produce SO^+, SO_2^+, SO_3^+, HSO_3^+, and $H_2SO_4^+$ fragments and SOCs only can produce SO^+ and SO_2^+ fragments (Supplementary Note 2), this suggested the existence of SOCs and its distribution with RH[3]. This was consistent with the mass concentration of SOCs gradually increased as a function of RH in Fig. 3b and the distribution of $f_{HSO_3^+}$ vs. $f_{H_2SO_4^+}$ scatters with higher RH were closer to SOCs in Fig. 3c [41]. Besides, the $f_{HSO_3^+}$ vs. $f_{H_2SO_4^+}$ of the standard compounds AS, methanesulfonic acid (MSA), and SOCs referred from Chen et al. [41] form a clear triangular distribution in Fig. 3c, which facilitates species identification from the scatters measured during the observations. The observation illustrated SOCs formation mostly occurred under the condition of high RH and was driven by the aqueous-phase process. Meanwhile, SO^+/HSO_3^+, $SO^+/H_2SO_4^+$, SO_2^+/HSO_3^+, and $SO_2^+/H_2SO_4^+$ in the haze period were larger than those measured from AS standard, also indicating the SOCs formation, particularly before snow (Supplementary Table 2).

The mass concentration of SOCs was abundant during observation, which was higher than the total average concentration of organosulfates captured in Beijing in summer 2016[23], but lower than SOCs in winter 2015[42]. However, the species of them remained indistinct. According to the previous observation in haze episodes, the possible species may include methanesulfonic acid (MSA), hydroxymethanesulfonate (HMS), sulfones, and organosulfates[28,43,44]. However, the presence of MSA, HMS, sulfones was trace or insignificant in our observation (Supplementary Note 2), although several studies have suggested that HMS was predominant in the distribution of SOCs during winter in Beijing[43,45,46]. The variation in HMS was mainly due to the significantly lower concentration of HCHO (3.8 ppb) compared to previous years (7.7 ppb in winter 2014[47] and ~20 ppb in winter 2015[45]).

As shown in Fig. 4a, glycolic acid sulfate (GAS) may be the dominant SOCs species during entire haze period including haze episodes before rain and snow due to the good correlation between SOCs and glyoxal-related fragments ($CH_2O_2^+$: $r^2 = 0.66$, $p < 0.01$; $C_2H_2O_2^+$: $r^2 = 0.84$, $p < 0.01$; and $C_2O_2^+$: $r^2 = 0.76$, $p < 0.01$). It was consistent with that GAS was the abundant species among measured organosulfates during the Beijing haze in previous reports[23,28]. The reported production of GAS through acid-catalyzed mechanism that glyoxal is first hydrolyzed and protonated, and then reacts with either sulfuric acid, sulfate or hydrogen sulfate[24]. $ALWC[CH_2O_2^+][SO_4^{2-}]$, $ALWC[C_2H_2O_2^+][SO_4^{2-}]$ and $ALWC[C_2O_2^+][SO_4^{2-}]$, standing for the aqueous-phase formation of GAS, correlated well with SOCs before rain (Fig. 4b, $r^2 = 0.37$–0.76, $p < 0.01$) and before snow (Fig. 4c, $r^2 = 0.51$–0.98, $p < 0.01$) both during daytime and at night, indicating the significance of this pathway for atmospheric SOCs. In addition, SOCs after snow correlated significantly with those factors at night ($r^2 = 0.53$–0.93, $p < 0.01$), suggesting that SOCs after snow was mainly achieved by nightly GAS aqueous-phase accumulation.

Furthermore, according to the significant correlation between SOCs with aromatic species (benzene: $r^2 = 0.91$, toluene: $r^2 = 0.93$ and naphthalene: $r^2 = 0.93$, $p < 0.01$) during morning of November 3rd (6:00–12:00) and monoterpene ($r^2 = 0.82$, $p < 0.05$) during daytime of November 4th, it can be deduced that aromatic and monoterpene contributed to SOCs through photochemical processing. It had been reported that aromatic species can

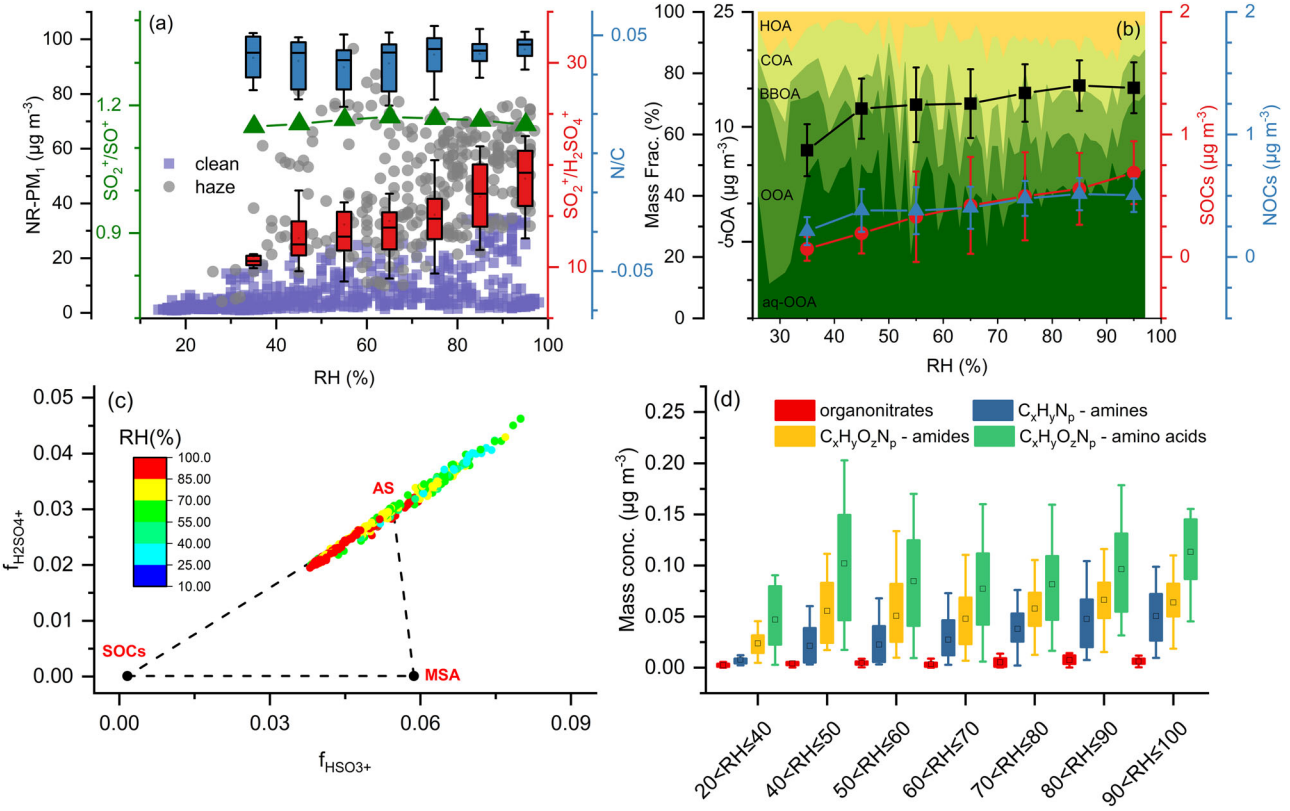

Fig. 3 | Variations of chemical species and related ratios as a function of RH. **a** Mass concentration of NR-PM_1 during entire observation and the ratios of SO_2^+/SO^+, $SO_2^+/H_2SO_4^+$ and N/C during haze periods; **b** Mass fraction distribution of OA factors, the mass concentration of OA, SOCs and NOCs; **c** The triangle plot of $f_{HSO_3^+}$ versus $f_{H_2SO_4^+}$ during haze periods (The fragments information $f_{HSO_3^+}$ versus $f_{H_2SO_4^+}$ of AS, MSA and SOCs referred to Chen et al. [41]); **d** Mass concentrations of organonitrates, total mass concentrations of amines species fragments (CH_4N^+, $C_2H_6N^+$, $C_3H_8N^+$, $C_4H_{10}N^+$, and $C_5H_{12}N^+$), amides species fragments (CH_2NO^+, $C_2H_4NO^+$, $C_3H_6NO^+$, and $C_4H_8NO^+$), and amino acids species fragments (CH_4NO^+, $C_2H_3NO^+$, and $C_2H_4NO_2^+$) with increasing RH. For the box diagram, the upper and lower edge lines are the maximum and minimum values, the upper and lower boundaries of the box are the 75th and 25th percentiles, the horizontal line in the middle of the box is the median, and the hollow square inside the box is the mean value.

react to form a series of organosulfates in the presence of UV light on acidic or neutral ammonium sulfate particles[48], and monoterpene-derived SOCs can be produced by the reaction of monoterpene species, especially α-/β-pinene, with •OH radicals or O_3 under acidic or strongly acidic sulfate seed aerosol conditions[25,26,49].

$UV[O_3]$ and O_X were treated as •OH radical proxies representing the photochemical activity of the atmospheric environment[50,51]. $UV[O_3][SO_4^{2-}]$ was used to stand for the photochemical process of monoterpene-derived SOCs production[50]. Figure 4b showed that •OH radicals from solar-excited O_3 act on monoterpene-derived SOCs production prior to rainfall, but its contribution was limited because of poor correlation between SOCs and monoterpene (Fig. 4a). Photochemical process represented by O_X contributed significantly to haze events prior to snowfall, especially on November 4th, while the impact was limited after snowfall. Besides, $\bullet NO_3$ radical represented by $[NO_2][O_3]$, which can react with biogenic VOCs (BVOCs) to form nitrooxy organosulfates through nocturnal chemistry[26], contributed little to SOCs before and after both precipitation events.

As shown in Fig. 3a, the ratio of N/C exhibited an increasing trend when RH was greater than 60%, indicating that high RH environment was favorable to NOCs generation. Atmospheric NOCs consists mainly of amines, amino acids, amides, organonitrates, nitriles, nitro- and N-heterocyclic compounds, and more[52–54]. According to related characteristic fragments and extrapolation formula, amines ($C_nH_{2n+2}N^+$, $n = 1, 2, 3, 4, 5 \ldots$), amides ($C_nH_{2n}NO^+$, $n = 1, 2, 3, 4 \ldots$), amino acids (CH_4NO^+, $C_2H_3NO^+$, $C_2H_4NO_2^+$) and organonitrates ($RONO_2$) were detected in this observation, as shown in Fig. 3d. Within each RH interval, the four NOCs mass concentrations were ranked as amino acids > amides > amines > organonitrates; only amines species increased with increasing RH, while amino acids, amides and organonitrates peaked at 40% < RH < 50%, and all three increased as a function of RH at RH > 60%. The oxidation degree of amines, amides, amino acids, and organonitrates is gradually increasing. The highest percentage of amino acids indicated that secondary NOCs with a higher oxidation degree were dominant species during haze periods. Nevertheless, this was contrary to the result with primary NOCs emitted from biomass burning shared mostly in Beijing urban winter haze reported by Xu et al. [52], while the variation trend of NOCs in our study aligned with that of aq-OOA (Fig. 3b), indicating a dominance of secondary generation.

As shown in Fig. 4d, the significant correlation during haze daytime was observed between NOCs and amides species CH_2NO^+ ($r^2 = 0.85$, $p < 0.01$), which can originate from urea, pyrazinecarboxamide, and L-asparagine[54]. Despite the good correlations observed between NOCs and each species during clean periods ($r^2 = 0.35–0.87$, $p < 0.01$), the mass concentrations of NOCs were notably low. Before the rain, the amines species $C_3H_8N^+$, representing tertiary amines, exhibited good correlation with NOCs during daytime ($r^2 = 0.65$, $p < 0.01$), while the amides species $C_4H_8NO^+$ correlated well with NOCs during nighttime ($r^2 = 0.70$, $p < 0.01$). Additionally, VOC species, including isoprene, benzene, toluene, and naphthalene, showed significant correlations with NOCs at night ($r^2 = 0.96–0.99$, $p < 0.01$), suggesting their potential role as precursors. Before the snow, amides species CH_2NO^+ and amino acids species $C_2H_3NO^+$, such as serine, valine, cysteine, and leucine[54], correlated well with NOCs during daytime ($r^2 = 0.84$ and 0.81, $p < 0.01$). Additionally, significant correlations between NOCs and amides (CH_2NO^+: $r^2 = 0.95$, $p < 0.01$; $C_2H_4NO^+$: $r^2 = 0.95$, $p < 0.01$), amino acids

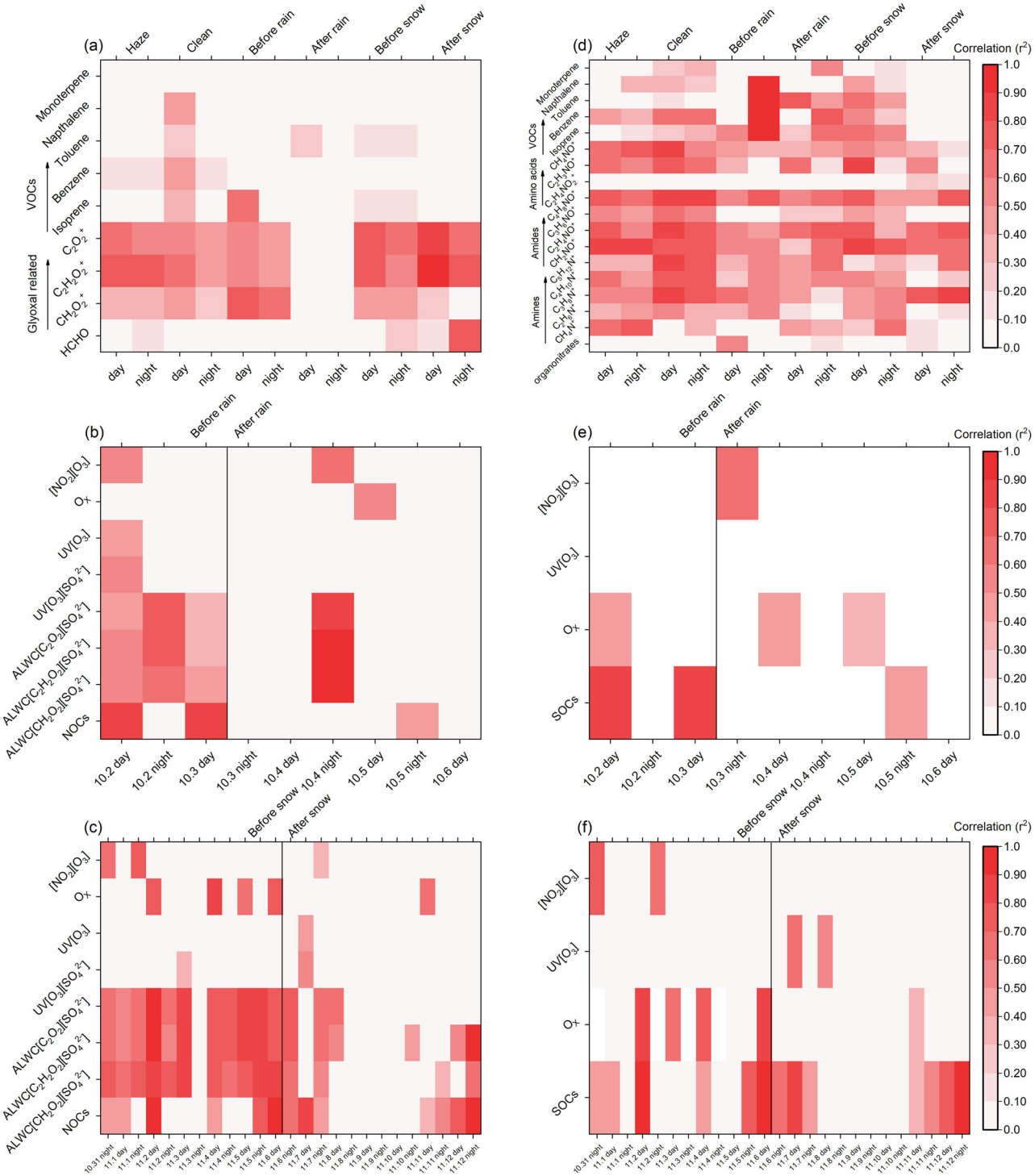

Fig. 4 | Correlation (r^2) between SOCs and NOCs with related elements. **a** Possible precursors of SOCs, **b**, **c** Formation pathways of SOCs during rain episode and snow episode; **d** NOCs compositions and possible precursors of NOCs, **e**, **f** Formation pathways of NOCs during rain episode and snow episode. Possible precursors of SOCs included HMS related specie (HCHO), glyoxal-related fragments ($CH_2O_2^+$, $C_2O_2^+$ and $C_2H_2O_2^+$), VOCs (isoprene, benzene, toluene, naphthalene and monoterpene); and possible formation pathways of SOCs included glyoxal-related factors ($ALWC[CH_2O_2^+][SO_4^{2-}]$, $ALWC[C_2H_2O_2^+][SO_4^{2-}]$ and $ALWC[C_2O_2^+][SO_4^{2-}]$), VOCs related factor ($UV[O_3][SO_4^{2-}]$), photochemical factors ($UV[O_3]$ and O_X) and nocturnal $\bullet NO_3$ radicals ($[NO_2][O_3]$). NOCs compositions included organonitrates, amines species, amides species and amino acids species, and possible precursors mainly included VOCs; and possible formation pathways of NOCs included photochemical factors ($UV[O_3]$ and O_X) and nocturnal $\bullet NO_3$ radicals ($[NO_2][O_3]$). The figure shows the squared values of the Pearson correlation coefficients and the colored sections all pass the significance test.

($C_2H_3NO^+$: $r^2 = 0.92$, $p < 0.01$) and isoprene ($r^2 = 0.94$, $p < 0.01$) on 3rd November daytime (7:00–15:00), indicating the photochemical processing of related NOCs species.

The evolution of NOCs was attributed to the oxidation of VOCs by •OH or $•NO_3$ radicals to form gas-phase NOCs, with semi-volatile gas-phase NOCs transferring into the particulate phase through gas-particle partitioning or oxidation[17,31,36,53]. As shown in Fig. 4e, NOCs well correlated with O_X before rain ($r^2 = 0.40$, $p < 0.05$) and with $•NO_3$ radical after rain ($r^2 = 0.62$, $p < 0.01$), which indicated the different processes before and after rainfall. The difference was that during snow episode in Fig. 4f, NOCs well correlated with O_X during daytime ($r^2 = 0.63$–0.87, $p < 0.01$) and $•NO_3$ radical during night ($r^2 = 0.63$–0.74, $p < 0.01$) before snowfall, while correlated with UV[O_3] during daytime ($r^2 = 0.59$–0.68, $p < 0.01$) after snow. This suggested that O_3 played crucial roles in the formation of NOCs, regardless of whether it was through daytime photochemical processing or nighttime formation promoted by $•NO_3$ radicals.

Generally, in addition to the direct effect of wet scavenging, the chemical formation mechanisms of SOCs and NOCs played important roles in the transformation of their dominance before and after precipitation. GAS formed by the aqueous-phase pathway under high ALWC conditions dominated the pre-precipitation SOCs, also accompanied by aromatic- and monoterpene-derived SOCs formed by the photochemical pathway under UV irradiation and high O_3 conditions. Whereas the abundance of SOCs was negligible after precipitation. For NOCs, photochemical pathway was the main pathway with the assistance of O_3 both before and after precipitation. Therefore, favorable aqueous-phase reaction conditions before precipitation for SOCs and superior photochemical reaction conditions after precipitation for NOCs contributed to the transformation of them.

Methods

Instrumentation and measurements

The observation site was located on the rooftop of the 8th floor of the environmental technology building at the Research Center for Eco-Environment Science (RCEES, 40.0°N, 116.3°E), Chinese Academy of Sciences. The field observation was carried out from 1st October to 12th November 2021. NR-PM_1 (non-refractory submicron aerosol species, i.e., organics, sulfate, nitrate, ammonium, and chloride) was measured by using an Aerodyne high-resolution time-of-flight aerosol mass spectrometer (HR-ToF-AMS, hereafter AMS, Aerodyne Research Inc., USA). Detailed information of AMS has been described previously in the literature[55]. A collection efficiency factor (CE) of 0.5 was estimated using the algorithm based on the aerosol chemical composition to calculate the mass concentration[55,56]. The relative ionization efficiency values (RIE) for nitrate, sulfate, chloride, and OA were 1.1, 1.2, 1.3, and 1.4, respectively[55,57]. The RIE value of NH_4^+ was 4.0, which was determined using the pure ammonium nitrate (NH_4NO_3) particles[55].

The $PM_{2.5}$ mass concentrations were obtained from the measurements at the state control station Olympic Center, which is about 5 km from our sampling site. The concentrations of VOCs species, including isoprene, benzene, toluene, naphthalene, and monoterpene were measured by a proton transfer reaction time-of-flight mass spectrometer (PTR-ToF-MS, hereafter PTR, Ionicon Analytik GmbH, Austria). Gaseous pollutants concentrations including sulfur dioxide (SO_2), nitrogen dioxide (NO_2) and nitrogen oxides (NO_x), carbon monoxide (CO), and ozone (O_3) were monitored by gas analyzers (model 43i, model 42i-TL, model 48i, and model 49i, respectively, Thermo Scientific, USA). The mixing ratio of formaldehyde (HCHO) was detected by a Picarro G2307 (Picarro, USA) gas concentration analyzer. NH_3 was measured by a Quantum Cascade Tunable Infrared Laser Differential Absorption Spectrometer (QCTILDAS, Aerodyne Research, USA). The meteorological parameters including relative humidity (RH), temperature (T), wind speed (WS), and wind direction (WD) were also measured at the same site with a weather station (Vaisala Inc., Finland). The ultraviolet radiation (UV, 290–400 nm) was detected by CUV3 broad band UV radiometer (Kipp & Zonen, the Netherlands), which can record radiation data at 1 min intervals.

Data analysis

The airflow trajectories and cluster analysis of air masses before and after two precipitations were analyzed by backward trajectory based on the Hybrid Single-Particle Lagrangian Integrated Trajectory (HYSPLIT, version 5) model and Global Data Assimilation System (GDAS). 48-h back trajectories were calculated in this study at four times (0:00, 6:00,12:00, and 18:00 UTC) each day, and the starting height of the trajectory selected in this study was 50 m above the surface ground.

The mass concentrations of NR-PM_1 species and elemental ratios of OA were obtained by analyzing AMS data using the high-resolution data analysis packages (PIKA V1.25 G) in Igor Pro (Version 8.04, Wavemetrics Inc., USA). The mass concentration of NR-PM_1 species was obtained by the sum of OA, sulfate, nitrate, ammonium, and chloride mass concentration. After data processing, fragments related to SOCs species were extracted, primarily comprising SO^+, SO_2^+, SO_3^+, HSO_3^+, and $H_2SO_4^+$. Similarly, extracted fragments related to NOCs included amines ($C_nH_{2n+2}N^+$, $n = 1, 2, 3, 4, 5$ …), amides ($C_nH_{2n}NO^+$, $n = 1, 2, 3, 4$ …), amino acids (CH_4NO^+, $C_2H_3NO^+$, $C_2H_4NO_2^+$). Although NOCs can generate significant levels of NH_x^+ and NO_x^+ ion fragments, these ions are generally considered to be representative of inorganic nitrogen species[54]. Therefore, the use of relevant ion fragments to analyze NOCs was abandoned in this study. High-resolution mass spectra of OA were used to perform source apportionment using the PMF software tool (PMF Evaluation Tool, PET, version 2.06). In summary, five OA factors were identified based on the detailed feature fragments and diagnostic plots (details can be found in Supplementary Information), including two secondary OA (OOA, and aq-OOA), and three primary OA (HOA, COA, and BBOA). Hydrogen to carbon (H/C), oxygen to carbon (O/C), and organic aerosol to organic carbon (OA/OC) were calculated by the "Improved-Ambient" method[58]. Nitrogen to carbon (N/C) and sulfur to carbon (S/C) were calculated by "Aiken-Ambient" method[59,60].

The method reported by Song et al. [43] was utilized to estimate SOCs mass concentration, which was based on the assumption that SOCs only generate SO^+ and SO_2^+ fragments[43]:

$$\mathrm{SOCs} = M_{SO_4^{2-}} \times \left[\frac{SO^+_{obs} - R_{cd,SO^+/H_ySO_x^+} \times H_ySO^+_{x,obs}}{M_{SO^+}} + \frac{SO^+_{2,obs} - R_{cd,SO_2^+/H_ySO_x^+} \times H_ySO^+_{x,obs}}{M_{SO_2^+}}\right] \quad (1)$$

where SO^+_{obs} and $SO^+_{2,obs}$ are the observed mass concentrations of SO^+ and SO_2^+; M_{SO^+}, $M_{SO_2^+}$ and $M_{SO_4^{2-}}$ are the molar masses of SO^+, SO_2^+ and SO_4^{2-}, respectively; $R_{cd,SO^+/H_ySO_x^+}$ and $R_{cd,SO_2^+/H_ySO_x^+}$ are the average ratios of $SO^+/H_ySO_x^+$ and $SO_2^+/H_ySO_x^+$ during clean and dry periods (NR-$PM_1 < 2\ \mu g\ m^{-3}$ and RH < 20% in this study).

The mass concentration of NOCs, including amines, amides, amino acids, organonitrates, and more, was estimated through the ratios of OA/OC and N/C as below[52]:

$$\mathrm{NOCs} = \frac{OA_{mass}}{\mathrm{OA/OC}} \times \left(\frac{\mathrm{N}}{\mathrm{C}}\right) \times \left(\frac{14}{12}\right) \quad (2)$$

In addition, the mass fraction and concentration of particulate organonitrates were calculated as below[61]:

$$\mathrm{Organonitrates_{frac}} = \frac{(1 + R_{OrgNO3}) \times (R_{measured} - R_{calib})}{(1 + R_{measured}) \times (R_{OrgNO3} - R_{calib})} \quad (3)$$

$$\mathrm{Organonitrates_{mass}} = \mathrm{Organonitrates_{frac}} \times NO_{3,total} \quad (4)$$

where R_{OrgNO3} is the value of NO_2^+/NO^+ for organonitrates set to 0.1, which is the minimum value in the field observation data[61]; $R_{measured}$ is the measured intensity ratio of NO_2^+/NO^+ during our observation; and R_{calib} is the

ratio of NO_2^+/NO^+ observed in NH_4NO_3 calibrations with the range of 0.29–0.49 and used in this study as 0.4[61].

The estimation ALWC was the sum of the water associated with the inorganic components (W_i) and organic components (W_o). W_i was calculated by the thermodynamic model of ISORROPIA II[62]. The ISORROPIA II model was operated in the forward mode because of its low sensitivity to measurement errors[63,64]. W_o was calculated by the simplified equation based on the k-Köhler theory[65]. NH_3 concentration was used in the forward model. The detailed information about the calculation process has been introduced in the previous report[66].

Data availability

The data that support the findings of this study are available from the authors on reasonable request.

Received: 4 April 2024; Accepted: 26 August 2024;
Published online: 04 September 2024

References

1. Guo, S. et al. Elucidating severe urban haze formation in China. *Proc. Natl Acad. Sci. USA* **111**, 17373–17378 (2014).
2. Sun, Y. et al. Chemical characteristics of $PM_{2.5}$ and PM_{10} in haze-fog episodes in Beijing. *Environ. Sci. Technol.* **40**, 3148–3155 (2006).
3. Zhao, J. et al. Organic aerosol processing during winter severe haze episodes in Beijing. *J. Geophys. Res. Atmos.* **124**, 10248–10263 (2019).
4. Li, Y. J. et al. Real-time chemical characterization of atmospheric particulate matter in China: a review. *Atmos. Environ.* **158**, 270–304 (2017).
5. Huang, X. F. et al. Highly time-resolved chemical characterization of atmospheric submicron particles during 2008 Beijing Olympic Games using an Aerodyne High-Resolution Aerosol Mass Spectrometer. *Atmos. Chem. Phys.* **10**, 8933–8945 (2010).
6. Elser, M. et al. New insights into $PM_{2.5}$ chemical composition and sources in two major cities in China during extreme haze events using aerosol mass spectrometry. *Atmos. Chem. Phys.* **16**, 3207–3225 (2016).
7. Sun, Y. et al. Primary and secondary aerosols in Beijing in winter: sources, variations and processes. *Atmos. Chem. Phys.* **16**, 8309–8329 (2016).
8. Hu, W. et al. Seasonal variations in high time-resolved chemical compositions, sources, and evolution of atmospheric submicron aerosols in the megacity Beijing. *Atmos. Chem. Phys.* **17**, 9979–10000 (2017).
9. Hu, R. et al. Variations and sources of organic aerosol in winter Beijing under markedly reduced anthropogenic activities during COVID-2019. *Environ. Sci. Technol.* **56**, 6956–6967 (2022).
10. Wang, Y. H. et al. Aerosol physicochemical properties and implications for visibility during an intense haze episode during winter in Beijing. *Atmos. Chem. Phys.* **15**, 3205–3215 (2015).
11. Xiao, Y. et al. Insights into aqueous-phase and photochemical formation of secondary organic aerosol in the winter of Beijing. *Atmos. Environ.* **259**, 118535 (2021).
12. Zhou, W. et al. A review of aerosol chemistry in Asia: insights from aerosol mass spectrometer measurements. *Environ. Sci. Proc. Imp.* **22**, 1616–1653 (2020).
13. Wang, Y. et al. Contrasting trends of $PM_{2.5}$ and surface-ozone concentrations in China from 2013 to 2017. *Natl Sci. Rev.* **7**, 1331–1339 (2020).
14. Shrivastava, M. et al. Urban pollution greatly enhances formation of natural aerosols over the Amazon rainforest. *Nat. Commun.* **10**, 1046 (2019).
15. Kourtchev, I. et al. Enhanced volatile organic compounds emissions and organic aerosol mass increase the oligomer content of atmospheric aerosols. *Sci. Rep.* **6**, 35038 (2016).
16. Ervens, B. et al. Secondary organic aerosol formation in cloud droplets and aqueous particles (aqSOA): a review of laboratory, field and model studies. *Atmos. Chem. Phys.* **11**, 11069–11102 (2011).
17. Wang, Y. et al. Molecular composition of oxygenated organic molecules and their contributions to organic aerosol in Beijing. *Environ. Sci. Technol.* **56**, 770–778 (2022).
18. Chen, T. et al. Synergistic effects of SO_2 and NH_3 coexistence on SOA formation from gasoline evaporative emissions. *Environ. Sci. Technol.* **57**, 6616–6625 (2023).
19. McNeill, V. F. Aqueous organic chemistry in the atmosphere: Sources and chemical processing of organic aerosols. *Environ. Sci. Technol.* **49**, 1237–1244 (2015).
20. Zhan, B. et al. The roles of aqueous-phase chemistry and photochemical oxidation in oxygenated organic aerosols formation. *Atmos. Environ.* **266**, 118738 (2021).
21. Duan, J. et al. Summertime and wintertime atmospheric processes of secondary aerosol in Beijing. *Atmos. Chem. Phys.* **20**, 3793–3807 (2020).
22. Xu, L. et al. Chemical characterization of water-soluble organic aerosol in contrasting rural and urban environments in the southeastern United States. *Environ. Sci. Technol.* **51**, 78–88 (2017).
23. Wang, Y. et al. The secondary formation of organosulfates under interactions between biogenic emissions and anthropogenic pollutants in summer in Beijing. *Atmos. Chem. Phys.* **18**, 10693–10713 (2018).
24. Liggio, J. et al. Heterogeneous reactions of glyoxal on particulate matter: identification of acetals and sulfate esters. *Environ. Sci. Technol.* **39**, 1532–1541 (2005).
25. Surratt, J. D. et al. Organosulfate formation in biogenic secondary organic aerosol. *J. Phys. Chem. A* **112**, 8345–8378 (2008).
26. Iinuma, Y. et al. Evidence for the existence of organosulfates from β-pinene ozonolysis in ambient secondary organic aerosol. *Environ. Sci. Technol.* **41**, 6678–6683 (2007).
27. Darer, A. I. et al. Formation and stability of atmospherically relevant isoprene-derived organosulfates and organonitrates. *Environ. Sci. Technol.* **45**, 1895–1902 (2011).
28. Le Breton, M. et al. Online gas- and particle-phase measurements of organosulfates, organosulfonates and nitrooxy organosulfates in Beijing utilizing a FIGAERO ToF-CIMS. *Atmos. Chem. Phys.* **18**, 10355–10371 (2018).
29. Xie, Q. et al. Increase of high molecular weight organosulfate with intensifying urban air pollution in the megacity Beijing. *J. Geophys. Res. Atmos.* **125**, e2019JD032200 (2020).
30. Ma, Y. et al. Seasonal and diurnal variations of particulate organosulfates in urban Shanghai, China. *Atmos. Environ.* **85**, 152–160 (2014).
31. Nie, W. et al. Secondary organic aerosol formed by condensing anthropogenic vapours over China's megacities. *Nat. Geosci.* **15**, 255–261 (2022).
32. Koenig, T. K. et al. Particulate organic nitrogen observed in wintertime Beijing haze by FIGAERO-I-CIMS, December 01, 2022, A24E-01 (2022).
33. Garmash, O. et al. Multi-generation OH oxidation as a source for highly oxygenated organic molecules from aromatics. *Atmos. Chem. Phys.* **20**, 515–537 (2020).
34. Perring, A. E. et al. An observational perspective on the atmospheric impacts of alkyl and multifunctional nitrates on ozone and secondary organic aerosol. *Chem. Rev.* **113**, 5848–5870 (2013).
35. Ng, N. L. et al. Nitrate radicals and biogenic volatile organic compounds: oxidation, mechanisms, and organic aerosol. *Atmos. Chem. Phys.* **17**, 2103–2162 (2017).
36. Rollins, A. W. et al. Evidence for NOx control over nighttime SOA formation. *Science* **337**, 1210–1212 (2012).
37. Hu, W. et al. Chemical composition, sources, and aging process of submicron aerosols in Beijing: Contrast between summer and winter. *J. Geophys. Res. Atmos.* **121**, 1955–1977 (2016).

38. Zhang, Y. et al. Response of aerosol composition to different emission scenarios in Beijing, China. *Sci. Total Environ.* **571**, 902–908 (2016).
39. Sun, Y. L. et al. Long-term real-time measurements of aerosol particle composition in Beijing, China: seasonal variations, meteorological effects, and source analysis. *Atmos. Chem. Phys.* **15**, 10149–10165 (2015).
40. Zhang, J. K. et al. Characterization of submicron aerosols during a month of serious pollution in Beijing, 2013. *Atmos. Chem. Phys.* **14**, 2887–2903 (2014).
41. Chen, Y. et al. Response of the Aerodyne Aerosol Mass Spectrometer to inorganic sulfates and organosulfur compounds: applications in field and laboratory measurements. *Environ. Sci. Technol.* **53**, 5176–5186 (2019).
42. Wei, L. et al. Quantitative determination of hydroxymethanesulfonate (HMS) using Ion Chromatography and UHPLC-LTQ-Orbitrap Mass Spectrometry: a missing source of sulfur during haze episodes in Beijing. *Environ. Sci. Technol. Lett.* **7**, 701–707 (2020).
43. Song, S. et al. Possible heterogeneous chemistry of hydroxymethanesulfonate (HMS) in northern China winter haze. *Atmos. Chem. Phys.* **19**, 1357–1371 (2019).
44. Huang, S. et al. Latitudinal and seasonal distribution of particulate MSA over the Atlantic using a validated quantification method with HR-ToF-AMS. *Environ. Sci. Technol.* **51**, 418–426 (2016).
45. Ma, T. et al. Contribution of hydroxymethanesulfonate (HMS) to severe winter haze in the North China Plain. *Atmos. Chem. Phys.* **20**, 5887–5897 (2020).
46. Chen, C. et al. The importance of hydroxymethanesulfonate (HMS) in winter haze episodes in North China Plain. *Environ. Res.* **211**, 113093 (2022).
47. Rao, Z. et al. Carbonyl compounds over urban Beijing: concentrations on haze and non-haze days and effects on radical chemistry. *Atmos. Environ.* **124**, 207–216 (2016).
48. Riva, M. et al. Evidence for an unrecognized secondary anthropogenic source of organosulfates and sulfonates: Gas-phase oxidation of polycyclic aromatic hydrocarbons in the presence of sulfate aerosol. *Environ. Sci. Technol.* **49**, 6654–6664 (2015).
49. Nozière, B. et al. Radical-initiated formation of organosulfates and surfactants in atmospheric aerosols. *Geophys. Res. Lett.* **37**, L05806 (2010).
50. Yang, T. et al. Spatial and diurnal variations of aerosol organosulfates in summertime Shanghai, China: Potential influence of photochemical process and anthropogenic sulfate pollution. *EGUsphere* **2023**, 1–45 (2023).
51. Herndon, S. C. et al. Correlation of secondary organic aerosol with odd oxygen in Mexico City. *Geophys. Res. Lett.* **35**, L15804 (2008).
52. Xu, W. et al. Seasonal characterization of organic nitrogen in atmospheric aerosols using High Resolution Aerosol Mass Spectrometry in Beijing, China. *ACS Earth. Space Chem.* **1**, 673–682 (2017).
53. Farmer, D. K. et al. Response of an aerosol mass spectrometer to organonitrates and organosulfates and implications for atmospheric chemistry. *Proc. Natl Acad. Sci. USA* **107**, 6670–6675 (2010).
54. Ge, X. et al. Enhancing characterization of organic nitrogen components in aerosols and droplets using high-resolution aerosol mass spectrometry. *Atmos. Meas. Tech.* **17**, 423–439 (2024).
55. Chen, T. et al. Chemical characterization of submicron aerosol in summertime Beijing: a case study in southern suburbs in 2018. *Chemosphere* **247**, 125918 (2020).
56. Middlebrook, A. M. et al. Evaluation of composition-dependent collection efficiencies for the Aerodyne Aerosol Mass Spectrometer using field data. *Aerosol Sci. Tech.* **46**, 258–271 (2012).
57. Jimenez, J. L. et al. Ambient aerosol sampling using the Aerodyne Aerosol Mass Spectrometer. *J. Geophys. Res. Atmos.* **108**, 8425 (2003).
58. Canagaratna, M. R. et al. Elemental ratio measurements of organic compounds using aerosol mass spectrometry: characterization, improved calibration, and implications. *Atmos. Chem. Phys.* **15**, 253–272 (2015).
59. Aiken, A. C. et al. Mexico City aerosol analysis during MILAGRO using high resolution aerosol mass spectrometry at the urban supersite (T0) – Part 1: fine particle composition and organic source apportionment. *Atmos. Chem. Phys.* **9**, 6633–6653 (2009).
60. Aiken, A. C. et al. O/C and OM/OC ratios of primary, secondary, and ambient organic aerosols with High-Resolution Time-of-Flight Aerosol Mass Spectrometry. *Environ. Sci. Technol.* **42**, 4478–4485 (2008).
61. Kiendler-Scharr, A. et al. Ubiquity of organic nitrates from nighttime chemistry in the European submicron aerosol. *Geophys. Res. Lett.* **43**, 7735–7744 (2016).
62. Li, X. et al. Interactions between aerosol organic components and liquid water content during haze episodes in Beijing. *Atmos. Chem. Phys.* **19**, 12163–12174 (2019).
63. Hennigan, C. J. et al. A critical evaluation of proxy methods used to estimate the acidity of atmospheric particles. *Atmos. Chem. Phys.* **15**, 2775–2790 (2015).
64. Song, S. et al. Fine-particle pH for Beijing winter haze as inferred from different thermodynamic equilibrium models. *Atmos. Chem. Phys.* **18**, 7423–7438 (2018).
65. Lambe, A. T. et al. Laboratory studies of the chemical composition and cloud condensation nuclei (CCN) activity of secondary organic aerosol (SOA) and oxidized primary organic aerosol (OPOA). *Atmos. Chem. Phys.* **11**, 8913–8928 (2011).
66. Huang, W. et al. Exploring the inorganic and organic nitrate aerosol formation regimes at a suburban site on the North China Plain. *Sci. Total. Environ.* **768**, 144538 (2021).

Acknowledgements

This study was supported by the National Natural Science Foundation of China (42205098, 22188102, and 22376206).

Author contributions

C.Z.: Investigation, Formal analysis, Writing - original draft, Writing - review & editing. Y.W.: Conceptualization, Supervision, Writing - review & editing. J.L.: Formal analysis, Writing - review & editing. T.C.: Writing - review & editing. W.H.: Data curation, Writing - review & editing. Z.L.: Data curation, Writing - review & editing. B.C.: Writing - review & editing. Q.M.: Writing - review & editing. H.H.: Supervision, Resources, Writing - review & editing.

Competing interests

The authors declare no competing interests.

Additional information

Supplementary information The online version contains supplementary material available at https://doi.org/10.1038/s41612-024-00756-5.

Correspondence and requests for materials should be addressed to Yonghong Wang or Hong He.